Metabolomic analysis of *Drosophila melanogaster* larvae lacking Pyruvate kinase

Authors

Yasaman Heidarian[1], Jason P. Tourigny[1], Tess D. Fasteen[1], Nader H. Mahmoudzadeh[1], Alexander J. Hurlburt[1], Travis Nemkov[2], Julie A. Reisz[2], Angelo D'Alessandro[2], and Jason M. Tennessen[1]

Affiliations

[1]Department of Biology, Indiana University, Bloomington, IN 47405, USA

[2]Department of Biochemistry and Molecular Genetics, Anschutz Medical Campus, University of Colorado School of Medicine, Aurora, CO 80045, USA

ABSTRACT

Pyruvate kinase (Pyk) is a rate-limiting enzyme that catalyzes the final metabolic reaction in glycolysis. The importance of this enzyme, however, extends far beyond ATP production, as Pyk is also known to regulate tissue growth, cell proliferation, and development. Studies of this enzyme in *Drosophila melanogaster*, however, are complicated by the fact that the fly genome encodes six Pyk paralogs whose functions remain poorly defined. To address this issue, we used sequence distance and phylogenetic approaches to demonstrate that the gene *Pyk* encodes the enzyme most similar to the mammalian Pyk orthologs, while the other five *Drosophila* Pyk paralogs have significantly diverged from the canonical enzyme. Consistent with this observation, metabolomic studies of two different *Pyk* mutant backgrounds revealed that larvae lacking Pyk exhibit a severe block in glycolysis, with a buildup of glycolytic intermediates upstream of pyruvate. However, our analysis also unexpectedly reveals that steady state pyruvate levels are unchanged in *Pyk* mutants, indicating that larval metabolism maintains pyruvate pool size despite severe metabolic limitations. Consistent with our metabolomic findings, a complementary RNA-seq analysis revealed that genes involved in lipid metabolism and peptidase activity are elevated in *Pyk* mutants, again indicating that loss of this glycolytic enzyme induces compensatory changes in other aspects of metabolism. Overall, our study provides both insight into how Drosophila larval metabolism adapts to disruption of glycolytic metabolism as well as immediate clinical relevance, considering that Pyk deficiency is the most common congenital enzymatic defect in humans.

INTRODUCTION

The enzyme Pyruvate kinase (Pyk; E.C. 2.7.1.40) catalyzes the final reaction of glycolysis (phosphoenolpyruvate + ADP + Pi to pyruvate + ATP). Since the Pyk-catalyzed reaction is essentially irreversible under normal cellular conditions (SCHORMANN *et al.* 2019), this enzyme controls a key rate-limiting, "pay-off" glycolytic step that controls ATP production, and dictates the rate at which glycolytic intermediates enter the metabolic pathways that branch off both glycolysis and the TCA cycle. In so doing, Pyk regulates fluxes towards serine synthesis, which indirectly influences redox balance and nucleoside anabolism via the amino acids cysteine (de novo glutathione synthesis) and glycine (one-carbon metabolism for de novo purine synthesis) (MADDOCKS *et al.* 2013). Thus, changes in Pyk activity can influence cell growth, proliferation, and differentiation by balancing the flux of glycolytic metabolites between mitochondrial energy production and the synthesis of metabolites involved in chromatin remodeling, one-carbon metabolism, and biomass production (ISRAELSEN AND VANDER HEIDEN 2015; HSU AND HUNG 2018).

The importance of Pyk in human health is clear from the myriad of diseases that are caused by altered activity of the two human orthologs, Pyruvate Kinase, Liver and Red Blood Cell (PKLR) and Pyruvate Kinase, Muscle (PKM). For example, mutations in the *PKLR* gene result in a common congenital disorder known as Pyk deficiency (PKD) (FATTIZZO *et al.* 2022; LUKE *et al.* 2023). Individuals with PKD experience a wide spectrum of clinical and biochemical symptoms and have a highly variable prognoses that depend on environmental factors, early interventions, and the severity of the causal mutations (DOLAN *et al.* 2002; GRACE *et al.* 2015). Similarly, changes in splicing of PKM

62 transcripts are well-documented in a number of disease states, with a switch from the
63 PKM1 isoform towards the PKM2 isoform associated with pulmonary hypertension
64 (CARUSO *et al.* 2017; ZHANG *et al.* 2017), sporadic Alzheimer's disease (TRAXLER *et al.*
65 2022), and enhancement of the Warburg effect in cancer cells (ISRAELSEN AND VANDER
66 HEIDEN 2015). Finally, population genetic studies support a model in which *PKLR*
67 mutations are protective against malaria (MIN-OO *et al.* 2007; AYI *et al.* 2008; MACHADO *et*
68 *al.* 2012; VAN BRUGGEN *et al.* 2015), suggesting that partial inhibition of the enzyme could
69 be exploited toward anti-malarial efforts. Basic studies of PYK function in the context of
70 endogenous metabolic networks thus hold the potential to inform better interventions for
71 a wide range of human diseases.

72 The fruit fly *Drosophila melanogaster* is a powerful model for studying the
73 function of metabolic enzymes within the context of both normal physiology and human
74 disease models (DRUMMOND-BARBOSA AND TENNESSEN 2020; KIM *et al.* 2021). In this
75 regard, previous studies of *Drosophila* Pyk have demonstrated roles for this enzyme in
76 fly development and behavior, with reduced *Pyk* levels being associated with defects in
77 muscle and wing development, neuron and glial function, and olfactory memory (TIXIER
78 *et al.* 2013; VOLKENHOFF *et al.* 2015; WU *et al.* 2018; SPANNL *et al.* 2020). However, the
79 effects of decreased Pyk activity in the fly have not been examined at a metabolic level.
80 Moreover, the fly genome encodes six predicted Pyk paralogs (Pyk, CG7069, CG2964,
81 CG7362, CG11249, and CG12229,GARAPATI *et al.* 2019; GRAMATES *et al.* 2022b), thus
82 highlighting a need to characterize the *in vivo* functional potential of individual enzymes
83 within this gene class.

84 Here, we use sequence identities and phylogenetics in combination with
85 metabolomics and transcriptomics to analyze *Pyk* (FBgn0267385), which encodes the
86 most abundantly and widely expressed member of the *Drosophila melanogaster* Pyk
87 family (GRAVELEY *et al.* 2011). Our studies indicate that the gene *Pyk* encodes the
88 protein most analogous to the mammalian PKM and PKLR enzymes. Subsequent
89 metabolomic analysis of two genetically distinct *Pyk* mutant backgrounds reveals a
90 severe block in glycolysis, with a buildup of glycolytic intermediates and a depletion of
91 lactate, 2-hydroxyglutarate (2HG), and the amino acid proline. Moreover, the loss of Pyk
92 activity also induced a significant upregulation of genes involved in lipid metabolism and
93 protease activity. Overall, our study validates the presumed function of Pyk within
94 *Drosophila* metabolism and identifies the transcriptional and metabolic networks that
95 respond to loss of Pyk activity during larval development.

96 **METHODS**

97 ***Drosophila* husbandry and larval collection**

98 Fly stocks were maintained on Bloomington *Drosophila* Stock Center media at 25ºC.
99 Larvae were collected on molasses agar plates as previously described (LI AND
100 TENNESSEN 2017; LI AND TENNESSEN 2018). Briefly, 50 virgin females and 25 males of
101 the appropriate genotypes were placed in six-ounce plastic bottles (Genesee Scientific;
102 Cat #: 32-130) with holes punched in the side using a 20-gauge needle. A 35 mm
103 molasses agar plate (Corning 353001) with a smear of yeast paste on the surface was
104 taped in place in the mouth of the bottle and the bottle inverted and placed in a 25ºC
105 incubator. The molasses agar/yeast plate was replaced at least once per day. For
106 sample collection, eggs were collected on the molasses agar/yeast plate for 6 hours,
107 individual plates were placed inside a 60 mm cell culture dish, and the collected
108 embryos were placed in a 25ºC incubator and allowed to develop for 48 hours. Larvae
109 were collected at the early L2 stage for subsequent metabolomics analysis.

110

111 **Generation of *Pyk* alleles using CRISPR/Cas9**

112 The *Pyk* deletions Pyk^{23} and Pyk^{31} were generated using a previously described
113 approach for CRISPR/Cas9 mutagenesis (GRATZ *et al.* 2013; SEBO *et al.* 2014). Briefly,
114 oligos containing gRNA sequences #1 (5'- GTGCCCCATGTGCGTCTGTC-3') and #2
115 (5'- GCTGCTGGAGGCAGGTCCGA-3') were inserted into pU6-BbsI-chiRNA (DGRC
116 Stock #1362) and the resulting plasmids were independently injected into BDSC Stock
117 #52669 (y^1 *M{RFP[3xP3.PB] GFP[E.3xP3]=vas-Cas9.S}ZH-2A* w^{1118}) by Rainbow
118 Transgenics (Camarillo, CA). Injected females and F1 progeny were crossed to *w*;* ry^{506}

119 *Dr*^{1}*/TM3, P{Dfd-GMR-nvYFP}3, Sb*^{1}. Putative F2 *Pyk*$^{\Delta}$*/ TM3, P{Dfd-GMR-nvYFP}3, Sb*^{1}
120 siblings were mated and the F3 generation screened for animals lacking the *TM3*
121 balancer, indicating the presence of a lethal mutation. Any strain that failed to generate
122 homozygous mutant adults was crossed with *Pyk*^{61} mutants and the F1 progeny
123 analyzed for failure to complement. Mutant strains that failed to complement *Pyk*^{61} were
124 further analyzed for the presence of *Pyk* mutations. *Pyk*^{23} was isolated from injections
125 using gRNA#1 and *Pyk*^{31} was isolated from injections using gRNA#2. The deletions
126 were identified by amplifying and sequencing a region of the *Pyk* gene using oligos 5'-
127 CACGCACTTTGTTTACATCAGC-3' and 5'-GCACCAGTCCACGGTAGAGA-3'.
128

129 **Generation of *Pyk* alleles using p-element excision**

130 Both the *Pyk*^{60} *and Pyk*^{61} alleles were generated using standard techniques for
131 imprecise p-element excision (ROBERTSON *et al.* 1988; BELLEN *et al.* 2004). Briefly, virgin
132 females containing the transposon insertions *Pyk*^{DG05605}*/TM3, Sb*^{1}*, Ser*^{1} and
133 *Pyk*^{EY10213}*/TM3, Sb*^{1}*, Ser*^{1} (BDSC stock 20088) were independently crossed with *ry506*
134 *p{Δ2-3}99B* males. F1 virgin females lacking the TM3 balancer were crossed with *w*;*
135 *ry*^{506} *Dr*^{1}*/TM3, P{Dfd-GMR-nvYFP}3, Sb*^{1} males (BDSC stock 23231). F2 males with
136 white eyes were then crossed to *w*; ry*^{506} *Dr*^{1}*/TM3, P{Dfd-GMR-nvYFP}3, Sb*^{1} females
137 and F3 *Pyk*$^{\Delta}$*/ TM3, P{Dfd-GMR-nvYFP}3, Sb*^{1} siblings were used to establish mutant
138 lines. The *Pyk*^{60} allele was generated by the imprecise excision of *Pyk*^{EY21058} and the
139 *Pyk*^{61} deletion was generated by the imprecise excision of *Pyk*^{DG05605}. Endpoints of the
140 deletions were mapped using a PCR-based approach. The *Pyk*^{61} deletion was
141 sequenced by isolating homozygous mutant larvae, amplifying across the deletion using

142 the oligos 5'-GATTTCCTTCAGAGCATTTGCGTC-3' and 5'-
143 TTCACCGTGCAGCAAGACATC-3' and sequencing the resulting PCR product. The
144 *Pyk*^{61} deletion is 6400 bp long starting with the sequence 5'-
145 GATGCCTTTGTTGCCGCCCT-3' and ending with the sequence 5'-
146 GTATGAACTTCTCTCACGGC-3' and includes an 18 bp insertion of the sequence 5'-
147 AAGTTCAAGTTCTGGATT-3'. The *Pyk*^{60} allele represents a large deletion or
148 rearrangement between the sequences 5'-CTTCTGTTCTATCCGATTGCCGG-3' and
149 5'-TTGACGCGCTCATTGGGTTTC-3'. However, we were unable to produce a PCR
150 product spanning the lesion. The *Pyk*^{prec} allele is a precise excision of *Pyk*^{DG05605}. For all
151 analyses, the *Pyk*^{60}*/TM3, P{Dfd-GMR-nvYFP}3, Sb*^{1} *and Pyk*^{61}*/TM3, P{Dfd-GMR-*
152 *nvYFP}3, Sb*^{1} strains were crossed together and trans-heterozygous *Pyk*$^{60/61}$ mutant
153 larvae were selected for based on the absence of YFP.
154 Since the transposon excision events that produced the *Pyk*^{60} and *Pyk*^{61} deletion
155 alleles also disrupted neighboring genes, we further analyzed the effects of these
156 deletions on expression of neighboring genes. When these deletions are placed in
157 *trans*, the resulting heterozygote lacks sequence corresponding to nearly the entire *Pyk*
158 coding region and the 5' exons of the neighboring *Pyk* homolog *CG7069*. Northern blot
159 analysis of trans-heterozygous L2 larvae revealed that *Pyk*$^{60/61}$ larvae fail to accumulate
160 detectable *Pyk* mRNA transcripts (Figure S1). The mRNA of neighboring genes *Polr3F*
161 and *CG18596*, however, were present at similar levels in both *Pyk*^{Prec} and *Pyk*$^{60/61}$,
162 indicating that the phenotypes arising from the *Pyk* mutant background are specific to
163 loss of *Pyk* expression. Of note, the second pyruvate kinase homolog disrupted by
164 these deletions, *CG7069*, is not expressed during the embryonic and larval stages, and

since *Pyk*$^{60/61}$ larvae die prior to the L3 stage, the effects of these deletions on *CG7069* expression could not be examined.

Northern Blot Analysis

RNA was extracted from L2 larvae with TriPure isolation reagent and northern blot analysis was conducted as previously described (KARIM AND THUMMEL 1991; SULLIVAN AND THUMMEL 2003). The following PCR oligos were used to generate northern blot probes:

Pyk: 5'-GCTGACCACCAACAAGGAAT-3' and 5'-GCACCAGTCCACGGTAGAGA-3'

Polr3F: 5'-ACCAACGATGACCTGACCAAG-3' and 5'-ATTGTTTCCAGATCGGCCTCC-3'

rp49: 5'-ACAAATGTGTATTCCGACCACG-3' and 5'-TCAAGATGACCATCCGCCCAG-3'

Phylogenetic Analysis of Pyk orthologs and paralogs

Protein sequences for each of the Pyk homologs were retrieved from FlyBase (GRAMATES *et al.* 2022a), Saccharomyces Genome Database (ENGEL *et al.* 2014; WONG *et al.* 2023), WormBase (DAVIS *et al.* 2022), NCBI RefSeq (O'LEARY *et al.* 2016), TAIR (BERARDINI *et al.* 2015), and UniProt (2023). The longest verified isoform of each was selected for multiple sequence alignment (MSA; see Table S1 for protein sequence information), except for mosquito which was a predicted entry (PETCHAMPAI *et al.* 2019). For the sequence identity and similarity heatmaps, an ensemble MSA was performed via the M-Coffee web server (WALLACE *et al.* 2006; MORETTI *et al.* 2007; NGUYEN *et al.* 2015; MINH *et al.* 2020), running the default command: `t_coffee -

189 in=Pyk_homologs_E_coli_out.fa Mpcma_msa Mmafft_msa Mclustalw_msa
190 Mdialigntx_msa Mpoa_msa Mmuscle_msa Mprobcons_msa Mt_coffee_msa -
191 output=score_html clustalw_aln fasta_aln score_ascii phylip -tree -maxnseq=150 -
192 maxlen=2500 -case=upper -seqnos=off -outorder=input -run_name=result -
193 multi_core=4 -quiet=stdout'. The resulting MSA was analyzed using the `seqidentity()'
194 function of the Bio3D R package to extract pairwise matrices (GRANT *et al.* 2006), which
195 were visualized with corrplot (WEI AND V. 2021).
196 For the phylogenetic analysis, we first performed MSA with MAFFT v7.520 using
197 the E-INS-I algorithm to tolerate potentially large gaps between conserved segments
198 (KATOH AND STANDLEY 2013), with the command `mafft –maxiterate 1000 –thread 4 –
199 genafpair Pyk_homologs_incl_Aa_and_E_coli_outgroup.fa >
200 mafft_einsi_output.msa.fa'. We then reconstructed the phylogenetic tree with IQ-TREE
201 2 using the WAG model of protein substitution (WHELAN AND GOLDMAN 2001; NGUYEN *et*
202 *al.* 2015; HOANG *et al.* 2018; MINH *et al.* 2020), run with the command `iqtree2 -s
203 mafft_einsi_output.msa.fa –redo -B 1000 -T 4 -m WAG –prefix mafft_einsi_WAG'. The
204 resulting phylogeny was rooted to *E. coli*, formatted, and visualized using FigTree v1.4.4
205 (RAMBAUT 2018).
206
207 **Triglyceride Assays and Nile Red Staining**
208 Triglyceride levels in *Pyk* control and mutant L2 larvae were measured as
209 previously described (TENNESSEN *et al.* 2014). Briefly, synchronized populations of
210 embryos were collected for 4 hrs on a molasses agar plate with yeast paste smeared on
211 the surface, as described (LI AND TENNESSEN 2017). Embryos were allowed to hatch on

212 the surface of the collection plate and larvae were reared on the same plate in a 25 ºC
213 incubator. Sixty hours after egg-laying, heterozygous controls and homozygous mutant
214 larvae were identified based on lack of GFP expression from the *TM3, P{Dfd-GMR-*
215 *nvYFP}3, Sb*^{1} balancer chromosome. Twenty-five larvae of the appropriate genotypes
216 were then collected in 1.5 mL microfuge tubes, washed three times with phosphate-
217 buffered saline pH 7.0 (PBS), homogenized in 100 µl of cold PBS + 0.05% Tween 20
218 (PBST), and heat-treated for 10 min at 70ºC. The resulting homogenate was assayed
219 for triglyceride and soluble protein levels as previously described (TENNESSEN *et al.*
220 2014).
221 Nile red staining was conducted on L2 fat bodies as previously described
222 (GRÖNKE *et al.* 2005). Briefly, dissected tissues were fixed with 4% paraformaldehyde in
223 PBS for 30 min and washed with PBST three times for 5 minutes each, and then
224 incubated for 1 hr at room temperature in a 1:1000 dilution of Nile Red stock (10mg/mL
225 in acetone) in PBS. Tissues were washed three times for 5 minutes each in PBST,
226 mounted in Vectashield (Vector Laboratories), and imaged on a Leica SP8 Confocal at
227 568nm.
228
229 **Gas Chromatography Mass Spectrometry (GC-MS)-based Metabolomics**
230 *Pyk* mutant and control larvae were collected at the early L2 stage (~48 hours after egg-
231 laying at 25ºC) as previously described (LI AND TENNESSEN 2018). All samples collected
232 for analysis represent biological replicates obtained from independent mating bottles
233 and each sample contained 25 larvae. Analysis of the *Pyk*^{60} *and Pyk*^{61} alleles was
234 conducted by the University of Utah metabolomics core facility as previously described

235 (COX *et al.* 2017). *Pyk*$^{23/31}$ mutants and *Pyk*$^{23/+}$ control samples were analyzed by the
236 University of Colorado Metabolomics core facility. Data were normalized to sample
237 mass and internal standards.
238
239 **Ultra High-pressure Liquid Chromatography - Mass Spectrometry (UHPLC-MS)-**
240 **based Metabolomics** UHPLC-MS metabolomics analyses were performed at the
241 University of Colorado Anschutz Medical Campus, as previously described (NEMKOV *et*
242 *al.* 2019). Briefly, the analytical platform employs a Vanquish UHPLC system (Thermo
243 Fisher Scientific, San Jose, CA, USA) coupled online to a Q Exactive mass
244 spectrometer (Thermo Fisher Scientific, San Jose, CA, USA). The (semi)polar extracts
245 were resolved over a Kinetex C18 column, 2.1 x 150 mm, 1.7 µm particle size
246 (Phenomenex, Torrance, CA, USA) equipped with a guard column (SecurityGuard™
247 Ultracartridge – UHPLC C18 for 2.1 mm ID Columns – AJO-8782 – Phenomenex,
248 Torrance, CA, USA) using an aqueous phase (A) of water and 0.1% formic acid and a
249 mobile phase (B) of acetonitrile and 0.1% formic acid for positive ion polarity mode, and
250 an aqueous phase (A) of water:acetonitrile (95:5) with 1 mM ammonium acetate and a
251 mobile phase (B) of acetonitrile:water (95:5) with 1 mM ammonium acetate for negative
252 ion polarity mode. The Q Exactive mass spectrometer (Thermo Fisher Scientific, San
253 Jose, CA, USA) was operated independently in positive or negative ion mode, scanning
254 in Full MS mode (2 µscans) from 60 to 900 m/z at 70,000 resolution, with 4 kV spray
255 voltage, 45 sheath gas, 15 auxiliary gas. Calibration was performed prior to analysis
256 using the Pierce™ Positive and Negative Ion Calibration Solutions (Thermo Fisher
257 Scientific).

258

259 **Statistical Analysis of Metabolomics Data**

260 Both metabolomics datasets were analyzed using Metaboanalyst 5.0 (PANG *et al.*
261 2021), with data first preprocessed using log normalization and Pareto scaling.

262

263 **RNA-seq Analysis**

264 RNA from *Pyk*$^{23/+}$ heterozygous controls and *Pyk*$^{23/31}$ mutants was extracted from
265 L2 larvae with TriPure isolation reagent and further purified using a Qiagen RNeasy kit
266 (Catalog #74004). RNA-seq was performed on three whole-fly biological replicates for
267 *Pyk*$^{23/+}$ heterozygous controls and *Pyk*$^{23/31}$ mutants. Samples were paired-end
268 sequenced on the NextSeq 550 platform 75 cycles to a depth of 15-20 million reads
269 each, using standard Illumina TruSeq Stranded mRNA libraries, at the IU Center for
270 Genomics and Bioinformatics .

271 RNA-seq read quality was assessed with FastQC (ANDREWS 2010) and MultiQC
272 (EWELS *et al.* 2016), with adequate reads and no significant issues noted. Reads were
273 pseudo-aligned and quantified using Kallisto v0.46.0 (BRAY *et al.* 2016), the *D.*
274 *melanogaster* BDGP6.32 reference assembly and annotation retrieved through
275 Ensembl (CUNNINGHAM *et al.* 2022), and the gffread utility from the Cufflinks suite to
276 generate the transcriptome from the assembly and annotation (TRAPNELL *et al.* 2010).

277 Differential expression analysis was performed with DESeq2 v1.30.1 (LOVE *et al.*
278 2014) running in RStudio v1.4.1717 on R v4.0.4. Genes with average expression below
279 2 counts per sample (i.e. 48 counts per row) were filtered out before determining genes
280 with significant expression difference in at least one sample with the likelihood-ratio test
281 (LRT) and LRT p-value ≤ 0.05. Subsequent analysis and visualization were performed

282 in R using a variety of tools and packages. Correlation plots were generated using base
283 R and the corrplot package v0.92 (WEI AND SIMKO 2021). Principal components were
284 analyzed and visualized with PCAtools v2.2.0 (BLIGHE AND LUN 2022). Heatmaps,
285 including clustering analysis performed by the hclust method (from base R {stats}
286 package), were generated by pheatmap v1.0.12 (KOLDE 2019).
287 Gene Ontology Analysis was carried out using the GOrilla tool for genes that
288 were significantly (*P*-value <0.05) up-regulated or down-regulated by more than two-fold
289 in *Pyk* mutants (EDEN *et al.* 2009). Tissue enrichment analysis was conducted using
290 default settings for the "Preferred tissue (modEncode RNA_seq)" tool in PANGEA
291 version 1.1 beta (HU *et al.* 2023).
292
293 **Data Availability**
294 All strains and reagents are available upon request. All targeted metabolomics data
295 described herein are included in Tables S2 and S3. Processed RNA-seq data is
296 presented in Table S4 and available in NCBI Gene Expression Omnibus (GEO).
297

RESULTS

The *Drosophila* gene *Pyk* encodes the Pyk enzyme orthologous to human PKs

The *Drosophila* genome harbors six genes predicted to encode pyruvate kinases (GARAPATI *et al.* 2019; GRAMATES *et al.* 2022b). To better understand the relationships between the *Drosophila* Pyk paralogs and Pyk orthologs in other organisms, we compared their pairwise protein sequence identities and generated a phylogenetic gene tree to infer their evolutionary history (Figure 1, Table S1). Species examined included human and mouse, *Aedes aegypti, Caenorhabditis elegans*, *Saccharomyces cerevisiae*, and *Arabidopsis thaliana,* with *Escherichia coli* as the outgroup for tree rooting (Table S1). The pairwise sequence comparisons indicate that *Drosophila* Pyk shares strongest identity with that of the *Aedes aegypti* protein PK (XP_001649983.1), followed by those of its mammalian orthologs, the worm paralogs, and fly paralog CG7069 (Figure 1A). The other putative paralogs show identity to a lesser extent, with two of the *Drosophila* proteins (CG11249 and CG12229) displaying less than 20% identity with all other analyzed Pyk orthologs (Figure 1A). The sequence similarities, allowing for conservative residue substitutions, show a similar pattern (Figure S2). These results indicate that, at the sequence level, *Drosophila* Pyk is as or more similar to the yeast orthologs as it is to 4 of the 5 other putative fly paralogs.

Sequence distances may not correspond to actual evolutionary or functional relationships, so we next sought to reconstruct the Pyk gene tree using a maximum likelihood model of protein evolution. This phylogeny indicates that the *Drosophila* Pyk is sister to its *Aedes aegypti* ortholog (Figure 1B), which composes a larger clade with the more distantly related *Drosophila* paralogs. This insect Pyk/PK clade is in turn sister

322 to that of the mammalian orthologs, which share a common ancestor. We note strong
323 ultrafast bootstrap support for the insect and mammalian ortholog subclades, the yeast
324 and worm paralogs, and two pairs of the fly paralogs, with weak support for the fly
325 paralog internal branches and the relationships between species (Figure 1B).

326 *Aedes* PK1 was previously demonstrated to exhibit unique allosteric regulation
327 when compared with mammalian enzymes (PETCHAMPAI *et al.* 2019). Given the high
328 sequence similarity and close evolutionary relationship between these two Dipteran
329 proteins, our findings suggest that *Drosophila* Pyk functions in a similar manner to that
330 of mosquito PK. Overall, these results support the hypothesis that the fly gene *Pyk*
331 encodes the canonical glycolytic enzyme, which is consistent with previous studies
332 demonstrating that *Pyk* is the most widely expressed member of the *Drosophila*
333 *melanogaster* Pyk gene class (RUST AND COLLIER 1985; GRAVELEY *et al.* 2011).

334
335
336 **_Pyk_ mutants die during the second larval instar**

337 To determine how loss of Pyk activity affects *Drosophila* development, we used
338 CRISPR/Cas9 to generate two small deletions in the *Pyk* locus, Pyk^{23} and Pyk^{31}, both of
339 which induce frameshifts in the first coding exon and are predicted to be null alleles
340 (Figure 2A). When these two *Pyk* mutant alleles were placed in trans, the resulting
341 $Pyk^{23/31}$ mutants survived embryogenesis but died during the mid-L2 stage (Figure 2B).
342 Moreover, when compared with $Pyk^{23/+}$ heterozygous controls, *Pyk* mutants displayed a
343 significant decrease in both body mass and triglyceride stores (Figure 2C and 3A, B),
344 thus demonstrating that loss of Pyk activity significantly disrupts larval development. We
345 would note, however, that although *Pyk* mutants accumulate far less triglycerides (TAG)

346 than controls, the density of lipid droplets within the fat body as determined by Nile Red
347 staining (Figure 3A,B) remains similar to controls. Overall, these findings reveal that *Pyk*
348 mutant larvae exhibit many of the same phenotypes observed in *dERR* and *Pfk*
349 mutants, which also exhibit severe disruptions of glycolytic metabolism (RUST AND
350 COLLIER 1985; TENNESSEN *et al.* 2011).
351
352 **Metabolomic analysis of *Pyk* mutants**
353 To better understand how loss of *Pyk* alters larval metabolism, we used a
354 targeted metabolomics approach to compare $Pyk^{23/31}$ mutants with $Pyk^{23/+}$ heterozygous
355 controls during the L2 larval stage (Table S2). Partial Least Squares Discriminant
356 Analysis (PLS-DA) of the resulting data revealed that control and mutant samples
357 clustered in distinct groups (Figure S3). Subsequent analysis of the data revealed
358 increased levels of the metabolites immediately upstream of Pyk, 2/3-phosphoglycerate
359 and phosphoenolpyruvate, and a decrease in lactate, and 2-hydroxyglutarate, and most
360 amino acids that can be used as anaplerotic fuel in the citric acid cycle (Figure 4A-B,
361 Table S2). Overall, these changes are indicative of a block in glycolysis at the reaction
362 catalyzed by Pyk.
363 While the metabolite changes observed in our initial metabolomics dataset were
364 largely expected, we were surprised to find that steady state pyruvate levels were
365 unchanged in *Pyk* mutants (Table S2). To verify that pyruvate levels remained constant
366 even in the absence of Pyk, we analyzed a second series of *Pyk* mutants using a
367 different methodology in an independent metabolomics core facility. In this case, a
368 trans-heterozygous combination of two *Pyk* deletion alleles, $Pyk^{60/61}$, were compared

369 with a genetically-matched control strain that was homozygous for a precise excision
370 allele (Table S3; see Methods for a description of the alleles used). Although these
371 deletions also removed portions of *CG7069* (Figure 2A), which encodes another
372 member of the Pyk family, this gene is not expressed during most of larval
373 development, and thus our analysis likely reflects phenotypes caused by the loss of the
374 *Pyk* locus. Similar to the metabolomic profile of $Pyk^{23/31}$ mutants, $Pyk^{60/61}$ mutant L2
375 larvae exhibited increased levels of glycolytic metabolites immediately upstream of
376 pyruvate kinase activity (2-phosphoglycerate, 3-phosphoglycerate and
377 phosphoenolpyruvate), and decreased levels of the downstream metabolites lactate,
378 2HG, and several amino acids (Figure 5A,B; Table S3). Moreover, these *Pyk* mutant
379 larval samples also displayed normal pyruvate levels (Figure 5A), suggesting that
380 steady state levels of larval pyruvate are maintained by compensatory changes in other
381 metabolic pathways.
382 As an extension of our metabolomic studies, we compared our datasets to
383 identify those metabolites that were similarly altered in both *Pyk* mutant backgrounds.
384 While we would note that this comparative analysis is somewhat limited in that we used
385 two different targeted metabolomics protocols that were optimized to detect different
386 subsets of metabolites, molecules that appear in both analyses highlight metabolic
387 pathways that are significantly altered by loss of Pyk activity in different genetic
388 backgrounds. Despite the many metabolic changes observed in each individual dataset,
389 only a handful of metabolites were common among the two experiments: 2/3-
390 phosphoglycerate, phosphoenolpyruvate, lactate, 2-hydroxyglutarate, and proline
391 (Figure 6A-C). While the changes in 2/3-phosphoglycerate, phosphoenolpyruvate, and

392 lactate were to be expected, the decrease in 2HG and proline present an interesting
393 model for how metabolic flux could be rewired in the absence of Pyk activity. The
394 decrease in 2HG likely represents L-2HG, which is abundant in larvae (LI *et al.* 2017;
395 MAHMOUDZADEH *et al.* 2020). Since L-2HG is synthesized from α-ketoglutarate by LDH
396 and is sensitive to changes in lactate production (LI *et al.* 2017; LI *et al.* 2018), we
397 hypothesize that the decreased abundance of 2HG represents a smaller lactate pool
398 combined with a potential decrease in TCA cycle flux. Meanwhile, the decreased proline
399 levels present in *Pyk* mutants are quite informative because this amino acid is
400 commonly used by insects as an anaplerotic fuel for the TCA cycle (BURSELL 1981).
401 Based on this observation, future studies should determine if *Pyk* mutants are using
402 proline to sustain both pyruvate levels and early larval growth.
403
404 **Gene Expression Analysis of *Pyk* mutants**
405 Our metabolomic studies suggest that loss of Pyk activity induces compensatory
406 changes in other metabolic pathways that allow the larvae to survive early development.
407 To better understand if this metabolic rewiring is recapitulated at the level of gene
408 expression, we used RNA-seq to compare the expression profiles of $Pyk^{23/31}$ mutant
409 larvae with $Pyk^{23/+}$ heterozygous controls (Table S4). This analysis revealed significant
410 differences in the gene expression between mutant and control samples (Figure
411 S5A,B), with 755 genes up-regulated and 214 genes downregulated more than two-fold
412 in the *Pyk* mutant dataset (adjusted *P* value <= 0.05; Table S4, Figure 7). Notably, the
413 expression of the *Pyk* gene itself was down-regulated 8.3-fold when compared with the
414 control strain, thus demonstrating the severity of these deletion alleles (Table S4, Figure

415 7). The data also revealed a significant upregulation of the gene *Thor* (FBgn0261560),
416 the fly homolog of 4E-BP (BERNAL AND KIMBRELL 2000), which functions as a metabolic
417 brake that dampens mRNA translation (HAY AND SONENBERG 2004; TELEMAN *et al.*
418 2005). The significant upregulation of *Thor* transcript levels hints at one possible
419 mechanism by which *Pyk* mutants both rewire larval metabolism and slow growth in
420 response to a major metabolic insult.
421 To further analyze the *Pyk* mutant RNA-seq data, we used Gene Ontology (GO)
422 to better define the biological processes most affected by loss of Pyk activity (Figure
423 8A,B and Table S5). Our analysis revealed that *Pyk* mutant samples exhibited a
424 significant enrichment in GO categories associated with the digestion and metabolism of
425 chitin and glucosamines, lipids, and proteins (Figure 8A). Notably, analysis of the RNA-
426 seq data set using the "Preferred tissue" tool in PANGEA indicated that the digestive
427 system displays the largest number of significantly up-regulated genes in *Pyk* mutants
428 (Table S6) (HU *et al.* 2023), with many of the those genes being involved in lipid and
429 protein metabolism (Figure 8C). For example, lipid metabolism was the second-most
430 enriched GO category, and; most of the significantly up-regulated genes that fit within
431 this GO category encode intestinal lipases. Similarly, *Pyk* mutants exhibit significant
432 increases in genes that encode proteases (Figure 8A, C), many of which represent
433 digestive proteases predicted to be expressed within the intestine. Overall, our results
434 suggest that the metabolism of *Pyk* mutants attempts to compensate for its loss by
435 increasing expression of genes involved in the breakdown of macromolecules within the
436 digestive tract, perhaps as a means of increasing the uptake of dietary nutrients.
437

438 **DISCUSSION**

439 Here we demonstrate that *Pyk* mutants exhibit a larval lethal phenotype with
440 defects in larval growth and a severe block in glycolysis. While the phenotypic
441 consequences of mutating *Pyk* are largely expected, our study contains several
442 important findings for both the *Drosophila* and biomedical communities. First, we
443 demonstrate that while the *Drosophila* genome encodes several pyruvate kinase
444 orthologs, the gene *Pyk* encodes the canonical enzyme most analogous to Pyk in other
445 organisms. In fact, *Drosophila* Pyk is more similar to the two yeast orthologs than to the
446 other five pyruvate kinase orthologs present in the fly. Future studies should more
447 closely examine these paralogous enzymes and determine why *Drosophila*
448 *melanogaster* evolution produced such a specialized set of pyruvate kinases.

449 A second key finding from our sequence analysis is that *Drosophila* Pyk exhibits
450 nearly equivalent sequence similarity to both the mammalian PKLR and PKM orthologs.
451 This observation is important because PLKR and PKM are connected with distinct
452 disease phenotypes. Thus, future studies in the fly should be cautious when making
453 comparisons with disease states that are unique to either of the human enzymes.
454 Instead, the *Pyk* mutants should be used as a tool to understand how cells and tissues
455 respond to a general deficiency in Pyk activity, similar to previous studies that
456 manipulated *Drosophila* Pyk activity in imaginal disc development and neurons/glia
457 (TIXIER *et al.* 2013; VOLKENHOFF *et al.* 2015; WU *et al.* 2018; SPANNL *et al.* 2020). One
458 exciting possibility would be to use our newly described mutants as a background for
459 expressing disease causing variants of the human enzymes. After all, pyruvate kinase
460 deficiency is the most common enzymatic disorder detected in newborns, and
461 moreover, a wide variety of disease-causing PKLR variants have been identified (DOLAN

462 *et al.* 2002; GRACE *et al.* 2015; FATTIZZO *et al.* 2022; LUKE *et al.* 2023). Expression of the
463 wild-type and mutated enzyme variants in the fly would allow for a rapid genetic analysis
464 of how PKLR mutations alter cellular metabolism while also providing an *in vivo* platform
465 to test potential therapeutics.

466 Our studies of the *Pyk* mutant also reveal how a block in glycolysis alters
467 systemic metabolism in unexpected ways. Previous studies in the fly have examined
468 how disruption of glycolytic metabolism affects both the metabolome and transcriptome.
469 For example, the *Drosophila* Estrogen-Related Receptor (dERR) is a central regulator
470 of glycolytic metabolism throughout the fly lifecycle (TENNESSEN *et al.* 2011; BEEBE *et al.*
471 2020). Our studies reveal that the developmental defects exhibited by *Pyk* mutants
472 largely phenocopy those observed in *dERR* mutants although the *Pyk* and *dERR*
473 mutant metabolomic and transcriptomic profiles differ significantly. Unlike *dERR*
474 mutants, which display a buildup of sugars due to the down-regulated expression of
475 nearly every glycolytic enzyme (TENNESSEN *et al.* 2011; BEEBE *et al.* 2020), *Pyk* mutants
476 instead accumulate three glycolytic metabolites immediately upstream of the Pyk-
477 catalyzed reaction. Thus, our studies of *Pyk* highlight how the *dERR* mutant metabolic
478 profile represents a broad disruption of carbohydrate metabolism when compared with
479 the loss of a single *dERR* target gene.

480 While most aspects of the *Pyk* mutant metabolomics profile were expected based
481 on the known role of Pyk, several interesting observations emerged. First, steady state
482 levels of pyruvate were unchanged in *Pyk* mutants as compared with controls. Since the
483 other metabolites in glycolysis are changed in a manner that is indicative of a loss of
484 Pyk activity, and both lactate and TCA cycle intermediates exhibit a severe decrease,

485 flux into and out of the larval pyruvate pool must be severely compromised. Future
486 studies should explore this possibility using stable-isotope tracers and further examine
487 how larval metabolism maintains steady state pyruvate levels even under severe
488 metabolic stress.

489 Our analysis also raises questions about how *Pyk* mutants, as well as *dERR*
490 mutants, survive until the mid-L2 stage. Glycolysis is severely disrupted in both mutant
491 backgrounds, yet these animals continue to develop for almost three days when raised
492 under standard culture conditions. While this impressive resilience might be partially
493 explained by maternal loading of Pyk and other enzymes, both metabolomics and
494 transcriptomics analysis suggest that *Pyk* mutants switch fuel sources in an attempt to
495 maintain developmental progress. Notably, *Pyk* mutants exhibit a significant decrease in
496 the fermentation products lactate and 2HG, as well as a decrease in the amino acid
497 proline. All three changes signal a major reorganization of larval metabolism, as lactate
498 and L-2HG are present at high levels within normal larvae and represent pools of
499 carbon that are not immediately used for energy production and growth (LI *et al.* 2017).
500 Meanwhile, proline is commonly used for energy production in insects (TEULIER *et al.*
501 2016). Thus the depletion of lactate, 2HG, and proline steady state pools suggests that
502 *Pyk* mutant metabolism has become reliant on alternative energy sources, such as
503 proline, and lacks adequate resources to ferment pyruvate and α-ketoglutarate into
504 lactate and L-2HG, respectively. This hypothesis is also supported by RNA-seq
505 analysis, which uncovered a significant up-regulation of enzymes involved in the
506 digestion and metabolism of complex lipids and proteins. Overall, further studies of *Pyk*

507 mutants are warranted to understand how these metabolic adaptations are induced and
508 regulated.

509 Our results also revealed that *Pyk* mutants exhibit more severe developmental
510 phenotypes when compared with *Mpc1* mutants, which are unable to properly transport
511 pyruvate into the mitochondria (BRICKER *et al.* 2012). Considering that Pyk and Mpc1
512 both directly affect pyruvate metabolism, one might predict that mutations in these
513 genes would result in similar phenotypes. Instead, *Mpc1* mutants are viable when raised
514 on standard *Drosophila* media and only exhibit a lethal phenotype when placed on a
515 sugar-only diet (Bricker et al., 2012). Moreover, the metabolomics profile of *Mpc1* and
516 *Pyk* mutants display significant differences. Notably, serine levels are significantly
517 increased in *Mpc1* mutants – an observation that would be consistent with an
518 uncoupling of glycolysis and the TCA cycle causing a rerouting of glycolytic
519 intermediates into the serine/glycine biosynthetic pathway (Bricker et al.,2012). In contrast,
520 *Pyk* mutants exhibit no increase in serine production despite harboring very high levels
521 of 3-phosphoglycerate, which serves as the precursor for serine biosynthesis (YE *et al.*
522 2012). This difference is surprising because studies of PKM2 in cancer cells suggests
523 that decreased Pyk activity induces shunting of glycolytic intermediates into serine
524 production (YE *et al.* 2012).

525 One explanation for the dramatic phenotypic differences between *Pyk* and *Mpc1*
526 mutants stems from differences in lactate metabolism. Unlike *Pyk* mutants, *Mpc1*
527 mutants accumulate excess lactate. Thus, *Mpc1* mutants can generate two more ATPs
528 from each glucose molecule when compared with *Pyk* mutants, while also regenerating
529 ATP independent of mitochondrial activity. Future studies should test this model by

530 examining if *Mpc1;Ldh* double mutant exhibits metabolic and developmental
531 phenotypes that more closely mimic those observed in *Pyk* mutants.
532 In conclusion, we have here described a metabolomics profile of *Drosophila*
533 larvae lacking Pyk activity. While the resulting changes in central carbon metabolism
534 are largely expected, such an analysis of fly metabolism is essential as *Drosophila*
535 geneticists increasingly study the role of metabolism across a wide range of contexts.
536 Moreover, *Drosophila* metabolism is highly adaptable and compensates for metabolic
537 insult – as seen here by depletion of the anaplerotic amino acids proline, glutamate, and
538 glutamine. A careful exploration of these metabolic networks will be essential for
539 studying metabolism in the context of *Drosophila* growth, development, and models of
540 human disease.
541
542

543 **ACKNOWLEDGEMENTS**

544 Thanks to the Bloomington *Drosophila* Stock Center (NIH P40OD018537) for providing
545 fly stocks, the *Drosophila* Genomics Resource Center (NIH 2P40OD010949) for
546 genomic reagents, and Flybase (NIH 5U41HG000739). Metabolomics analysis
547 performed at the Metabolomics Core Facility at the University of Utah is supported by
548 spectrometry equipment obtained through NCRR Shared Instrumentation Grants
549 1S10OD016232-01, 1S10OD018210-01A1 and 1S10OD021505-01. Sequencing was
550 performed at Indiana University's Center for Genomics and Bioinformatics. All
551 computation was performed on Indiana University's Carbonate and Research Desktop
552 HPC clusters. We thank members of the Matt Hahn lab at IU for helpful guidance on the
553 phylogeny. J.M.T. is supported by the National Institute of General Medical Sciences of
554 the National Institutes of Health under a R35 Maximizing Investigators' Research Award
555 (MIRA; 1R35GM119557).

556

557 **FIGURE LEGENDS**

558 **Figure 1. Sequence identity and phylogeny of Pyk homologs.** (**A**) Heatmap of
559 pairwise sequence identities extracted from the ensemble MSA. (**B**) Phylogenetic
560 maximum likelihood gene tree. Ultrafast bootstrap support is shown on internal
561 branches. The dark grey highlighted clades include the canonical *Drosophila*
562 *melanogaster*, *Aedes aegypti*, and human/mouse orthologs, while the light grey region
563 encompasses the divergent fly paralogs. The tree is rooted to *E. coli* homolog PykA as
564 the outgroup. Species abbreviations: Aa, *A. aegypti; Dm*, *D. melanogaster*;
565 Hs, *H. sapiens*; Mm, *M. musculus*; Ce, *C. elegans*; Sc, *S. cerevisiae*; At, *A. thaliana*;
566 Ec, *E. coli.* See Supplemental Table 1 for a list of isoforms used in this analysis.

567

568 **Figure 2. Deletions in the *Pyk* coding region induce larval lethality and growth**
569 **defects.** (A) An illustration of the *Drosophila Pyk* locus and surrounding genes, as well
570 as the *Pyk* mutant alleles. The Pyk^{23} and Pyk^{31} alleles were generated using a
571 CRISPR/Cas9-based strategy and induce small deletions that result in frameshifts. The
572 Pyk^{60} and Pyk^{61} alleles represent deletions that remove the entire PYK coding region as
573 well as portions of neighboring genes. See Figure S1 for analysis of *Pol3f* and *CG7069*
574 gene expression in trans-heterozygous *Pyk* mutant backgrounds. (B) A histogram
575 illustrating the effects of *Pyk* mutations on larval viability. Note that nearly all $Pyk^{23/31}$
576 trans-heterozygous mutant animals die during the second larval instar – phenocopying
577 *dERR* mutants. $P<0.001$ (C) $Pyk^{23/31}$ mutants are significantly smaller than
578 heterozygous controls. n=6 samples containing 25 mid-L2 larvae. $^{**}P<0.01$. $^{***}P<0.001$.
579 *P*-values calculated using a Mann Whitney test.

580

581 **Figure 3. *Pyk* mutants exhibit decreased TAG levels.** TAG levels were assayed
582 during L2 development in *Pyk* mutants and heterozygous controls. (A) $Pyk^{23/31}$ mutants
583 exhibit significantly decreased triglycerides (TAG) as compared with $Pyk^{21/+}$ controls.
584 Data are normalized to soluble protein. n=6 biological replicates containing 25 mid-L2
585 larvae per sample. $^{**}P<0.01$. *P*-values calculated using a Mann Whitney test. (B,C) Nile
586 Red was used to stain lipid droplets in L2 fat bodies of both (B) $Pyk^{21/+}$ controls and (C)
587 $Pyk^{23/31}$ mutants. Scale bar in (B) applies to (C).

588

589 **Figure 4. Targeted metabolomic analysis of *Pyk* mutant larvae.** $Pyk^{23/31}$ mutant
590 larvae and $Pyk^{21/+}$ controls were analyzed using a targeted GC-MS approach. (A)
591 Differences in metabolite abundance between control and mutant samples are
592 represented as a volcano plot. Dashed vertical line represents a log2 fold change (FC)
593 of > 1.5. Dashed horizontal line represents $p < 0.01$. (B) A heat map illustrating the top
594 25 most significantly altered compounds in $Pyk^{23/31}$ mutants as compared with $Pyk^{21/+}$
595 controls. Both figures were generated using Metaboanalyst 5.0, as described in the
596 methods. Abbreviated compounds are 2/3-phosphoglycerate (2/3PG),
597 phosphoenolpyruvate (PEP), 2-hydroxyglutarate (2HG), 3-hydroxybutyrate (2HB), 5,10-
598 Methenyltetrahydrofolate (5,10-CH=THF), alanine (Ala), Asparagine (Asn), Glutamic
599 acid (Glu), Glutamine (Gln), 5'−Phosphoribosyl−N-formylglycinamide (FGAR), proline
600 (Pro), trehalose (Tre).

601

602 **Figure 5. Targeted metabolomic analysis of *Pyk* mutant larvae.** *Pyk*$^{60/61}$ mutant
603 larvae and precise excision controls (*Pyk*^{Prec}) were analyzed using a targeted GC-MS
604 approach. (A) Differences in metabolite abundance between control and mutant
605 samples are represented as a volcano plot. Dashed vertical line represents a fold
606 change (FC) of > 1.5. Dashed horizontal line represents $P < 0.01$. (B) A heat map
607 illustrating the top 25 most significantly altered compounds in *Pyk*$^{60/61}$ mutants as
608 compared with *Pyk*^{Prec} controls. Both figures were generated using Metaboanalyst 5.0,
609 as described in the methods. Abbreviated compounds are 3-phosphoglycerate (3PG),
610 2-phosphoglycerate (2PG), phosphoenolpyruvate (PEP), 2-hydroxyglutarate (2HG), 3-
611 hydroxybutyrate (2HB), alanine (Ala), Asparagine (Asn), Glutamic acid (Glu), Glutamine
612 (Gln), 5'−Phosphoribosyl−N-formylglycinamide (FGAR), proline (Pro), trehalose (Tre).
613
614 **Figure 6. A limited set of metabolites are significantly altered in both *Pyk* mutant**
615 **backgrounds.** (A) An illustration of glycolysis and the TCA cycle with metabolites that
616 are significantly altered in both *Pyk* mutant backgrounds highlighted in dark red (up-
617 regulated) and light blue (down-regulated). (B,C) Boxplots illustrating the change in
618 abundance of metabolites that are significantly altered in both (B) *Pyk*$^{60/61}$ and (C)
619 *Pyk*$^{23/31}$ mutant backgrounds. All boxplots were generated using Metaboanalyst 5.0, as
620 described in the methods. Black dots represent individual samples, the horizontal bar in
621 the middle represents the median and the yellow diamond represents the mean
622 concentration. For all boxplots, the metabolite fold-change was >2 fold and $P<0.01$.
623 Abbreviated compounds are 3-phosphoglycerate (3PG), 2-phosphoglycerate (2PG),
624 phosphoenolpyruvate (PEP), 2-hydroxyglutarate (2HG).

625

626 **Figure 7. RNA-seq analysis of *Pyk*$^{23/31}$ mutants as compared with *Pyk*$^{23/+}$ controls.**

627 A volcano plot illustrating gene expression changes in *Pyk*$^{23/31}$ mutants as compared

628 with *Pyk*$^{23/+}$ controls. Black vertical lines indicate absolute log fold change (LFC) ≥ 1.

629 Black horizontal line represents adjusted *P* value ≤ 0.05. The top 15 most significantly

630 changed genes are labeled, with all significant genes (abs(LFC) ≥ 1 and adj *p* ≤ 0.05)

631 shaded darker.

632

633 **Figure 8. Gene Ontology (GO) enrichment analysis of genes that are significantly**

634 **misregulated in *Pyk*$^{23/31}$ mutants.** GOrilla was used to determine GO enrichment

635 among those genes that were either (A) significantly up-regulated or (B) significantly

636 down-regulated in *Pyk*$^{23/31}$ mutants when compared to the *Pyk*$^{23/+}$ control. (C)

637 Significantly up-regulated genes in the GO categories “lipid metabolic process” and

638 “proteolysis” are grouped by enzymatic function, with the increased fold-change in gene

639 expression represented by a color gradient.

640

641

642 **SUPPLEMENTAL FIGURE LEGENDS**

643 **Figure S1. *Pyk* mRNA transcript levels are significantly reduced in *Pyk* mutant**
644 **larvae.** Total RNA from stage w^{1118}; Pyk^{prec} control larvae and w^{1118}; $Pyk^{60/61}$ mutant
645 larvae were analyzed by northern blot hybridization to detect transcripts encoding Pyk,
646 CG18596, and Polr3F. Hybridization to detect *rp49* mRNA is included as a loading
647 control.

648

649 **Figure S2. A comparison of sequence similarities between Pyk homologs.** A
650 heatmap of pairwise sequence identities extracted from the ensemble MSA. Species
651 abbreviations: Aa, *A. aegypti; Dm*, *D. melanogaster*; Hs, *H. sapiens*; Mm, *M. musculus*;
652 Ce, *C. elegans*; Sc, *S. cerevisiae*; At, *A. thaliana*; Ec, *E. coli.* See Supplemental Table
653 1 for a list of isoforms used in this analysis.

654

655 **Figure S3. A comparison of the metabolomic data from $Pyk^{23/31}$ mutant and $Pyk^{21/+}$**
656 **control samples using principal component (PC) analysis.** Targeted metabolomics
657 data from Table S1 was analyzed using principal component analysis. Analysis was
658 conducted using Metaboanalyst 5.0.

659

660 **Figure S4. A comparison of the metabolomic data from $Pyk^{60/61}$ mutant and Pyk^{prec}**
661 **control samples using principal component (PC) analysis.** Targeted metabolomics
662 data from Table S2 was analyzed using principal component analysis. Analysis was
663 conducted using Metaboanalyst 5.0.

664

665 **Figure S5. RNA-seq Principal Component Analysis and Correlations of**
666 **Experimental Replicates.** (A) PCA biplot of principal component 1 (PC1) versus PC2
667 for the top 5,000 genes by variance, with replicates labeled. (B) Spearman correlation
668 plot of the top 5,000 genes by variance after filtering out genes with either low/no
669 expression.
670

671 **SUPPLEMENTAL TABLE LEGENDS**

672 **Table S1.** Protein isoform information for the Pyk orthologs used in Figure 1 and Figure
673 S2.
674 **Table S2.** Metabolomic analysis of *Pyk*$^{23/31}$ mutants as compared with *Pyk*$^{23/+}$ controls.
675 **Table S3.** Metabolomic analysis of imprecise excision *Pyk* mutants as compared with
676 precise excision controls.
677 **Table S4.** RNA-seq results comparing gene expression between Pyk23/31 mutants and
678 *Pyk*$^{23/+}$.
679 **Table S5.** GO analysis of significantly mis-regulated genes from the RNAseq data
680 represented in Table S4 using GOrilla.
681 **Table S6.** Analysis of RNA-seq data from Table S4 using the Preferred tissue
682 (modEncode RNA_seq) tool in PANGEA.
683
684

LITERATURE CITED

2023 UniProt: the Universal Protein Knowledgebase in 2023. Nucleic Acids Res 51**:** D523-d531.

Andrews, S., 2010 FastQC: a quality control tool for high throughput sequence data., pp.

Ayi, K., G. Min-Oo, L. Serghides, M. Crockett, M. Kirby-Allen *et al.*, 2008 Pyruvate kinase deficiency and malaria. N Engl J Med 358**:** 1805-1810.

Beebe, K., M. M. Robins, E. J. Hernandez, G. Lam, M. A. Horner *et al.*, 2020 Drosophila estrogen-related receptor directs a transcriptional switch that supports adult glycolysis and lipogenesis. Genes Dev 34**:** 701-714.

Bellen, H. J., R. W. Levis, G. Liao, Y. He, J. W. Carlson *et al.*, 2004 The BDGP gene disruption project: single transposon insertions associated with 40% of Drosophila genes. Genetics 167**:** 761-781.

Berardini, T. Z., L. Reiser, D. Li, Y. Mezheritsky, R. Muller *et al.*, 2015 The Arabidopsis information resource: Making and mining the "gold standard" annotated reference plant genome. Genesis 53**:** 474-485.

Bernal, A., and D. A. Kimbrell, 2000 Drosophila Thor participates in host immune defense and connects a translational regulator with innate immunity. Proc Natl Acad Sci U S A 97**:** 6019-6024.

Blighe, K., and A. Lun, 2022 PCAtools: Everything Principal Components Analysis. R package version 2.8.0, pp.

Bray, N. L., H. Pimentel, P. Melsted and L. Pachter, 2016 Near-optimal probabilistic RNA-seq quantification. Nat Biotechnol 34**:** 525-527.

Bricker, D. K., E. B. Taylor, J. C. Schell, T. Orsak, A. Boutron *et al.*, 2012 A mitochondrial pyruvate carrier required for pyruvate uptake in yeast, Drosophila, and humans. Science 337**:** 96-100.

Bursell, E., 1981 The role of proline in energy metabolism, pp. 135-154 in *Energy metabolism in insects*. Springer.

Caruso, P., B. J. Dunmore, K. Schlosser, S. Schoors, C. Dos Santos *et al.*, 2017 Identification of MicroRNA-124 as a Major Regulator of Enhanced Endothelial Cell Glycolysis in Pulmonary Arterial Hypertension via PTBP1 (Polypyrimidine Tract Binding Protein) and Pyruvate Kinase M2. Circulation 136**:** 2451-2467.

Cox, J. E., C. S. Thummel and J. M. Tennessen, 2017 Metabolomic Studies in Drosophila. Genetics 206**:** 1169-1185.

Cunningham, F., J. E. Allen, J. Allen, J. Alvarez-Jarreta, M. R. Amode *et al.*, 2022 Ensembl 2022. Nucleic Acids Res 50**:** D988-d995.

Davis, P., M. Zarowiecki, V. Arnaboldi, A. Becerra, S. Cain *et al.*, 2022 WormBase in 2022-data, processes, and tools for analyzing Caenorhabditis elegans. Genetics 220.

Dolan, L. M., M. Ryan and J. Moohan, 2002 Pyruvate kinase deficiency in pregnancy complicated by iron overload. Bjog 109**:** 844-846.

Drummond-Barbosa, D., and J. M. Tennessen, 2020 Reclaiming Warburg: using developmental biology to gain insight into human metabolic diseases. Development 147.

730 Eden, E., R. Navon, I. Steinfeld, D. Lipson and Z. Yakhini, 2009 GOrilla: a tool for
731 discovery and visualization of enriched GO terms in ranked gene lists. BMC
732 Bioinformatics 10**:** 48.
733 Engel, S. R., F. S. Dietrich, D. G. Fisk, G. Binkley, R. Balakrishnan *et al.*, 2014 The
734 reference genome sequence of Saccharomyces cerevisiae: then and now. G3
735 (Bethesda) 4**:** 389-398.
736 Ewels, P., M. Magnusson, S. Lundin and M. Käller, 2016 MultiQC: summarize analysis
737 results for multiple tools and samples in a single report. Bioinformatics 32**:** 3047-
738 3048.
739 Fattizzo, B., F. Cavallaro, A. Marcello, C. Vercellati and W. Barcellini, 2022 Pyruvate
740 Kinase Deficiency: Current Challenges and Future Prospects. J Blood Med 13**:**
741 461-471.
742 Garapati, P. V., J. Zhang, A. J. Rey and S. J. Marygold, 2019 Towards comprehensive
743 annotation of Drosophila melanogaster enzymes in FlyBase. Database (Oxford)
744 2019.
745 Grace, R. F., A. Zanella, E. J. Neufeld, D. H. Morton, S. Eber *et al.*, 2015 Erythrocyte
746 pyruvate kinase deficiency: 2015 status report. Am J Hematol 90**:** 825-830.
747 Gramates, L. S., J. Agapite, H. Attrill, B. R. Calvi, M. A. Crosby *et al.*, 2022a FlyBase: a
748 guided tour of highlighted features. Genetics 220.
749 Gramates, L. S., J. Agapite, H. Attrill, B. R. Calvi, M. A. Crosby *et al.*, 2022b FlyBase: a
750 guided tour of highlighted features. Genetics 220.
751 Grant, B. J., A. P. Rodrigues, K. M. ElSawy, J. A. McCammon and L. S. Caves, 2006
752 Bio3d: an R package for the comparative analysis of protein structures.
753 Bioinformatics 22**:** 2695-2696.
754 Gratz, S. J., A. M. Cummings, J. N. Nguyen, D. C. Hamm, L. K. Donohue *et al.*, 2013
755 Genome engineering of Drosophila with the CRISPR RNA-guided Cas9
756 nuclease. Genetics 194**:** 1029-1035.
757 Graveley, B. R., A. N. Brooks, J. W. Carlson, M. O. Duff, J. M. Landolin *et al.*, 2011 The
758 developmental transcriptome of Drosophila melanogaster. Nature 471**:** 473-479.
759 Grönke, S., A. Mildner, S. Fellert, N. Tennagels, S. Petry *et al.*, 2005 Brummer lipase is
760 an evolutionary conserved fat storage regulator in Drosophila. Cell Metab 1**:** 323-
761 330.
762 Hay, N., and N. Sonenberg, 2004 Upstream and downstream of mTOR. Genes Dev 18**:**
763 1926-1945.
764 Hoang, D. T., O. Chernomor, A. von Haeseler, B. Q. Minh and L. S. Vinh, 2018
765 UFBoot2: Improving the Ultrafast Bootstrap Approximation. Mol Biol Evol 35**:**
766 518-522.
767 Hsu, M. C., and W. C. Hung, 2018 Pyruvate kinase M2 fuels multiple aspects of cancer
768 cells: from cellular metabolism, transcriptional regulation to extracellular
769 signaling. Mol Cancer 17**:** 35.
770 Hu, Y., A. Comjean, H. Attrill, G. Antonazzo, J. Thurmond *et al.*, 2023 PANGEA: A New
771 Gene Set Enrichment Tool for Drosophila and Common Research Organisms.
772 bioRxiv.
773 Israelsen, W. J., and M. G. Vander Heiden, 2015 Pyruvate kinase: Function, regulation
774 and role in cancer. Semin Cell Dev Biol 43**:** 43-51.

775 Karim, F. D., and C. S. Thummel, 1991 Ecdysone coordinates the timing and amounts
776 of E74A and E74B transcription in Drosophila. Genes Dev 5**:** 1067-1079.
777 Katoh, K., and D. M. Standley, 2013 MAFFT multiple sequence alignment software
778 version 7: improvements in performance and usability. Mol Biol Evol 30**:** 772-780.
779 Kim, S. K., D. D. Tsao, G. S. B. Suh and I. Miguel-Aliaga, 2021 Discovering signaling
780 mechanisms governing metabolism and metabolic diseases with Drosophila. Cell
781 Metab 33**:** 1279-1292.
782 Kolde, R., 2019 pheatmap: Pretty Heatmaps – an implementation of heatmaps that
783 offers more control over dimensions and appearance. (Version 1.0.12), pp.
784 Li, H., G. Chawla, A. J. Hurlburt, M. C. Sterrett, O. Zaslaver *et al.*, 2017 Drosophila
785 larvae synthesize the putative oncometabolite L-2-hydroxyglutarate during
786 normal developmental growth. Proc Natl Acad Sci U S A 114**:** 1353-1358.
787 Li, H., A. J. Hurlburt and J. M. Tennessen, 2018 A Drosophila model of combined D-2-
788 and L-2-hydroxyglutaric aciduria reveals a mechanism linking mitochondrial
789 citrate export with oncometabolite accumulation. Dis Model Mech 11.
790 Li, H., and J. M. Tennessen, 2017 Methods for studying the metabolic basis of
791 Drosophila development. Wiley Interdiscip Rev Dev Biol 6.
792 Li, H., and J. M. Tennessen, 2018 Preparation of Drosophila Larval Samples for Gas
793 Chromatography-Mass Spectrometry (GC-MS)-based Metabolomics. J Vis Exp.
794 Love, M. I., W. Huber and S. Anders, 2014 Moderated estimation of fold change and
795 dispersion for RNA-seq data with DESeq2. Genome Biol 15**:** 550.
796 Luke, N., K. Hillier, H. Al-Samkari and R. F. Grace, 2023 Updates and advances in
797 pyruvate kinase deficiency. Trends Mol Med 29**:** 406-418.
798 Machado, P., L. Manco, C. Gomes, C. Mendes, N. Fernandes *et al.*, 2012 Pyruvate
799 kinase deficiency in sub-Saharan Africa: identification of a highly frequent
800 missense mutation (G829A;Glu277Lys) and association with malaria. PLoS One
801 7**:** e47071.
802 Maddocks, O. D., C. R. Berkers, S. M. Mason, L. Zheng, K. Blyth *et al.*, 2013 Serine
803 starvation induces stress and p53-dependent metabolic remodelling in cancer
804 cells. Nature 493**:** 542-546.
805 Mahmoudzadeh, N. H., A. J. Fitt, D. B. Schwab, W. E. Martenis, L. M. Nease *et al.*,
806 2020 The oncometabolite L-2-hydroxyglutarate is a common product of dipteran
807 larval development. Insect Biochem Mol Biol 127**:** 103493.
808 Min-Oo, G., M. Tam, M. M. Stevenson and P. Gros, 2007 Pyruvate kinase deficiency:
809 correlation between enzyme activity, extent of hemolytic anemia and protection
810 against malaria in independent mouse mutants. Blood Cells Mol Dis 39**:** 63-69.
811 Minh, B. Q., H. A. Schmidt, O. Chernomor, D. Schrempf, M. D. Woodhams *et al.*, 2020
812 IQ-TREE 2: New Models and Efficient Methods for Phylogenetic Inference in the
813 Genomic Era. Mol Biol Evol 37**:** 1530-1534.
814 Moretti, S., F. Armougom, I. M. Wallace, D. G. Higgins, C. V. Jongeneel *et al.*, 2007 The
815 M-Coffee web server: a meta-method for computing multiple sequence
816 alignments by combining alternative alignment methods. Nucleic Acids Res 35**:**
817 W645-648.
818 Nemkov, T., J. A. Reisz, S. Gehrke, K. C. Hansen and A. D'Alessandro, 2019 High-
819 Throughput Metabolomics: Isocratic and Gradient Mass Spectrometry-Based
820 Methods. Methods Mol Biol 1978**:** 13-26.

821 Nguyen, L. T., H. A. Schmidt, A. von Haeseler and B. Q. Minh, 2015 IQ-TREE: a fast
822 and effective stochastic algorithm for estimating maximum-likelihood
823 phylogenies. Mol Biol Evol 32**:** 268-274.
824 O'Leary, N. A., M. W. Wright, J. R. Brister, S. Ciufo, D. Haddad *et al.*, 2016 Reference
825 sequence (RefSeq) database at NCBI: current status, taxonomic expansion, and
826 functional annotation. Nucleic Acids Res 44**:** D733-745.
827 Pang, Z., J. Chong, G. Zhou, D. A. de Lima Morais, L. Chang *et al.*, 2021
828 MetaboAnalyst 5.0: narrowing the gap between raw spectra and functional
829 insights. Nucleic Acids Res 49**:** W388-w396.
830 Petchampai, N., C. Murillo-Solano, J. Isoe, J. C. Pizarro and P. Y. Scaraffia, 2019
831 Distinctive regulatory properties of pyruvate kinase 1 from Aedes aegypti
832 mosquitoes. Insect Biochem Mol Biol 104**:** 82-90.
833 Rambaut, A., 2018 FigTree, pp.
834 Robertson, H. M., C. R. Preston, R. W. Phillis, D. M. Johnson-Schlitz, W. K. Benz *et al.*,
835 1988 A stable genomic source of P element transposase in Drosophila
836 melanogaster. Genetics 118**:** 461-470.
837 Rust, K. J., and G. E. Collier, 1985 Localization of a dosage sensitive region for
838 pyruvate kinase in Drosophila melanogaster. J Hered 76**:** 39-44.
839 Schormann, N., K. L. Hayden, P. Lee, S. Banerjee and D. Chattopadhyay, 2019 An
840 overview of structure, function, and regulation of pyruvate kinases. Protein Sci
841 28**:** 1771-1784.
842 Sebo, Z. L., H. B. Lee, Y. Peng and Y. Guo, 2014 A simplified and efficient germline-
843 specific CRISPR/Cas9 system for Drosophila genomic engineering. Fly (Austin)
844 8**:** 52-57.
845 Spannl, S., T. Buhl, I. Nellas, S. A. Zeidan, K. V. Iyer *et al.*, 2020 Glycolysis regulates
846 Hedgehog signalling via the plasma membrane potential. Embo j 39**:** e101767.
847 Sullivan, A. A., and C. S. Thummel, 2003 Temporal profiles of nuclear receptor gene
848 expression reveal coordinate transcriptional responses during Drosophila
849 development. Mol Endocrinol 17**:** 2125-2137.
850 Teleman, A. A., Y. W. Chen and S. M. Cohen, 2005 4E-BP functions as a metabolic
851 brake used under stress conditions but not during normal growth. Genes Dev 19**:**
852 1844-1848.
853 Tennessen, J. M., K. D. Baker, G. Lam, J. Evans and C. S. Thummel, 2011 The
854 Drosophila estrogen-related receptor directs a metabolic switch that supports
855 developmental growth. Cell Metab 13**:** 139-148.
856 Tennessen, J. M., W. E. Barry, J. Cox and C. S. Thummel, 2014 Methods for studying
857 metabolism in Drosophila. Methods 68**:** 105-115.
858 Teulier, L., J. M. Weber, J. Crevier and C. A. Darveau, 2016 Proline as a fuel for insect
859 flight: enhancing carbohydrate oxidation in hymenopterans. Proc Biol Sci 283.
860 Tixier, V., L. Bataillé, C. Etard, T. Jagla, M. Weger *et al.*, 2013 Glycolysis supports
861 embryonic muscle growth by promoting myoblast fusion. Proc Natl Acad Sci U S
862 A 110**:** 18982-18987.
863 Trapnell, C., B. A. Williams, G. Pertea, A. Mortazavi, G. Kwan *et al.*, 2010 Transcript
864 assembly and quantification by RNA-Seq reveals unannotated transcripts and
865 isoform switching during cell differentiation. Nat Biotechnol 28**:** 511-515.

Traxler, L., J. R. Herdy, D. Stefanoni, S. Eichhorner, S. Pelucchi *et al.*, 2022 Warburg-like metabolic transformation underlies neuronal degeneration in sporadic Alzheimer's disease. Cell Metab 34**:** 1248-1263.e1246.

van Bruggen, R., C. Gualtieri, A. Iliescu, C. Louicharoen Cheepsunthorn, P. Mungkalasut *et al.*, 2015 Modulation of Malaria Phenotypes by Pyruvate Kinase (PKLR) Variants in a Thai Population. PLoS One 10**:** e0144555.

Volkenhoff, A., A. Weiler, M. Letzel, M. Stehling, C. Klämbt *et al.*, 2015 Glial Glycolysis Is Essential for Neuronal Survival in Drosophila. Cell Metab 22**:** 437-447.

Wallace, I. M., O. O'Sullivan, D. G. Higgins and C. Notredame, 2006 M-Coffee: combining multiple sequence alignment methods with T-Coffee. Nucleic Acids Res 34**:** 1692-1699.

Wei, T., and V. Simko, 2021 R package 'corrplot': Visualization of a Correlation Matrix. (Version 0.92), pp.

Wei, T., and S. V., 2021 R package 'corrplot': Visualization of a Correlation Matrix., pp.

Whelan, S., and N. Goldman, 2001 A general empirical model of protein evolution derived from multiple protein families using a maximum-likelihood approach. Mol Biol Evol 18**:** 691-699.

Wong, E. D., S. R. Miyasato, S. Aleksander, K. Karra, R. S. Nash *et al.*, 2023 Saccharomyces genome database update: server architecture, pan-genome nomenclature, and external resources. Genetics 224.

Wu, C. L., C. C. Chang, J. K. Wu, M. H. Chiang, C. H. Yang *et al.*, 2018 Mushroom body glycolysis is required for olfactory memory in Drosophila. Neurobiol Learn Mem 150**:** 13-19.

Ye, J., A. Mancuso, X. Tong, P. S. Ward, J. Fan *et al.*, 2012 Pyruvate kinase M2 promotes de novo serine synthesis to sustain mTORC1 activity and cell proliferation. Proc Natl Acad Sci U S A 109**:** 6904-6909.

Zhang, H., D. Wang, M. Li, L. Plecitá-Hlavatá, A. D'Alessandro *et al.*, 2017 Metabolic and Proliferative State of Vascular Adventitial Fibroblasts in Pulmonary Hypertension Is Regulated Through a MicroRNA-124/PTBP1 (Polypyrimidine Tract Binding Protein 1)/Pyruvate Kinase Muscle Axis. Circulation 136**:** 2468-2485.

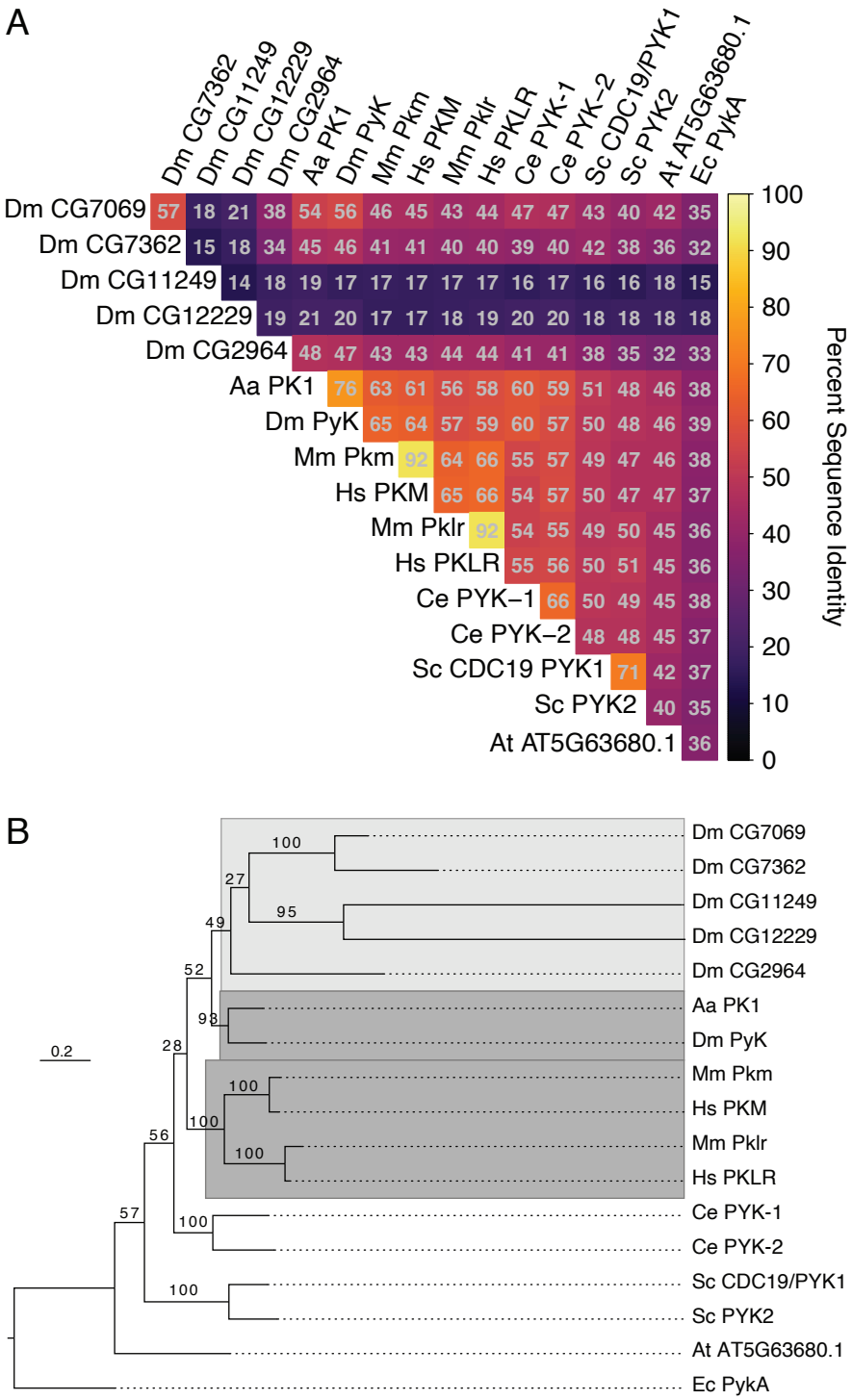

Figure 1. Sequence identity and phylogeny of Pyk homologs. (**A**) Heatmap of pairwise sequence identities extracted from the ensemble MSA. (**B**) Phylogenetic maximum likelihood gene tree. Ultrafast bootstrap support is shown on internal branches. The dark grey highlighted clades include the canonical *Drosophila melanogaster*, *Aedes aegypti*, and human/mouse orthologs, while the light grey region encompasses the divergent fly paralogs. The tree is rooted to *E. coli* homolog PykA as the outgroup. Species abbreviations: Aa, *A. aegypti; Dm*, *D. melanogaster*; Hs, *H. sapiens*; Mm, *M. musculus*; Ce, *C. elegans*; Sc, *S. cerevisiae*; At, *A. thaliana*; Ec, *E. coli.* See Supplemental Table 1 for a list of isoforms used in this analysis.

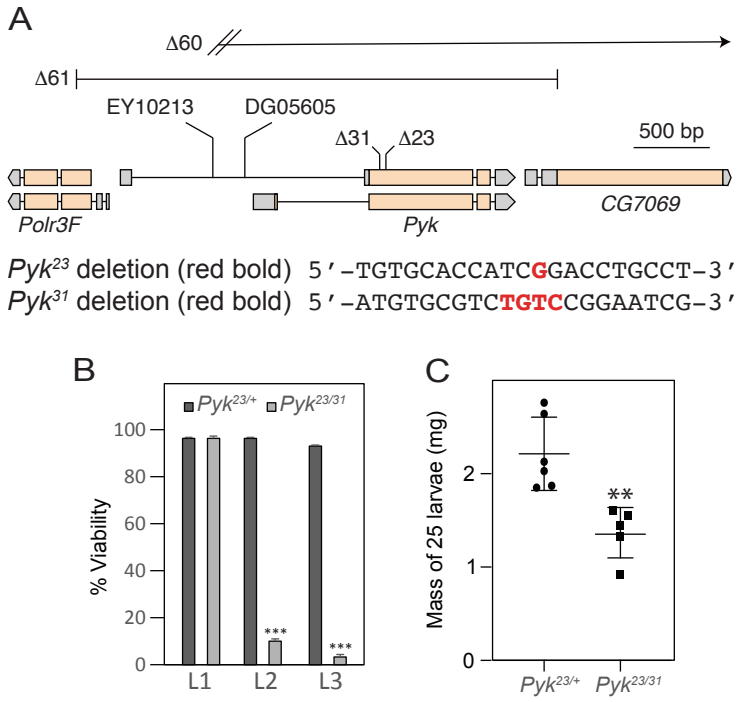

Figure 2. Deletions in the *Pyk* coding region induce larval lethality and growth defects. (A) An illustration of the *Drosophila Pyk* locus and surrounding genes, as well as the *Pyk* mutant alleles. The $Pyk^{23}$and Pyk^{31} alleles were generated using a CRISPR/Cas9-based strategy and induce small deletions that result in frameshifts. The Pyk^{60} and Pyk^{61} alleles represent deletions that remove the entire PYK coding region as well as portions of neighboring genes. See Figure S1 for analysis of *Pol3f* and *CG7069* gene expression in trans-heterozygous *Pyk* mutant backgrounds. (B) A histogram illustrating the effects of *Pyk* mutations on larval viability. Note that nearly all $Pyk^{23/31}$ trans-heterozygous mutant animals die during the second larval instar – phenocopying *dERR* mutants. $P<0.001$ (C) $Pyk^{23/31}$ mutants are significantly smaller than heterozygous controls. n=6 samples containing 25 mid-L2 larvae. $^{**}P<0.01$. $^{***}P<0.001$. *P*-values calculated using a Mann Whitney test.

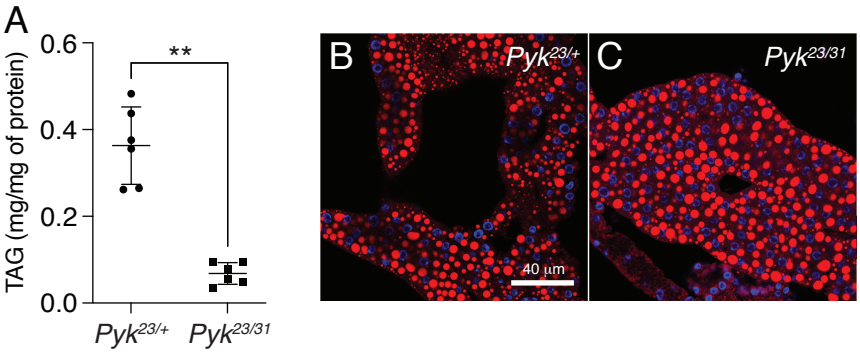

Figure 3. *Pyk* mutants exhibit decreased TAG levels. TAG levels were assayed during L2 development in *Pyk* mutants and heterozygous controls. (A) $Pyk^{23/31}$ mutants exhibit significantly decreased triglycerides (TAG) as compared with $Pyk^{21/+}$ controls. Data are normalized to soluble protein. n=6 biological replicates containing 25 mid-L2 larvae per sample. $^{**}P<0.01$. *P*-values calculated using a Mann Whitney test. (B,C) Nile Red was used to stain lipid droplets in L2 fat bodies of both (B) $Pyk^{21/+}$ controls and (C) $Pyk^{23/31}$ mutants. Scale bar in (B) applies to (C).

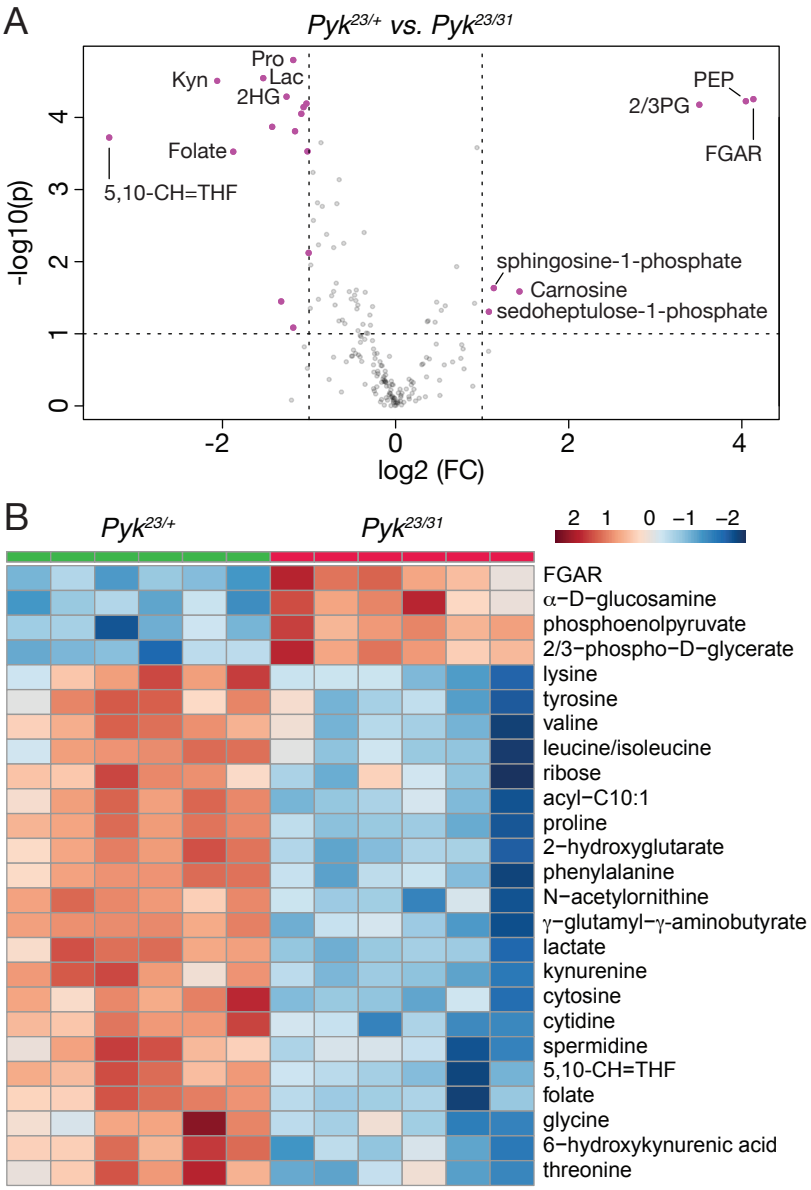

Figure 4. Targeted metabolomic analysis of *Pyk* mutant larvae. *Pyk*$^{23/31}$ mutant larvae and *Pyk*$^{21/+}$ controls were analyzed using a targeted GC-MS approach. (A) Differences in metabolite abundance between control and mutant samples are represented as a volcano plot. Dashed vertical line represents a log2 fold change (FC) of > 1.5. Dashed horizontal line represents $p < 0.01$. (B) A heat map illustrating the top 25 most significantly altered compounds in *Pyk*$^{23/31}$ mutants as compared with *Pyk*$^{21/+}$ controls. Both figures were generated using Metaboanalyst 5.0, as described in the methods. Abbreviated compounds are 2/3-phosphoglycerate (2/3PG), phosphoenolpyruvate (PEP), 2-hydroxyglutarate (2HG), 3-hydroxybutyrate (2HB), 5,10-Methenyltetrahydrofolate (5,10-CH=THF), alanine (Ala), Asparagine (Asn), Glutamic acid (Glu), Glutamine (Gln), 5'−Phosphoribosyl−N-formylglycinamide (FGAR), proline (Pro), trehalose (Tre).

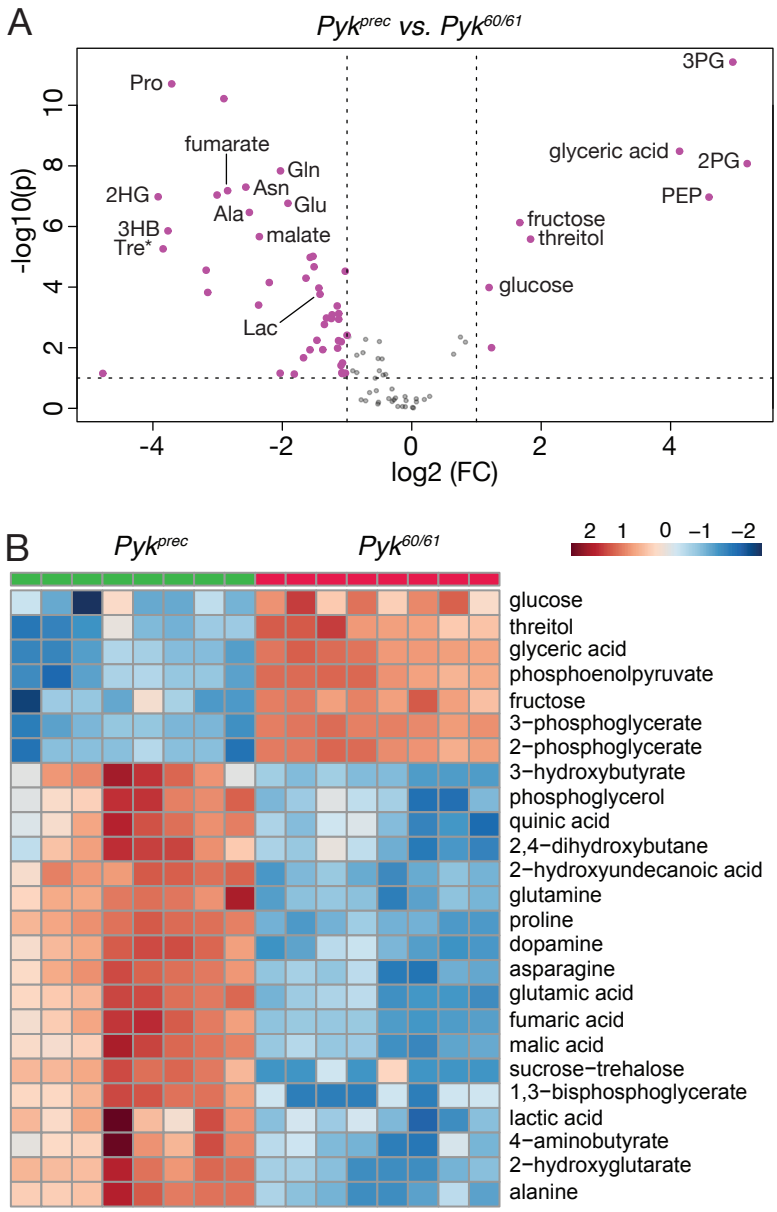

Figure 5. Targeted metabolomic analysis of *Pyk* mutant larvae. *Pyk*$^{60/61}$ mutant larvae and precise excision controls (*Pyk*^{Prec}) were analyzed using a targeted GC-MS approach. (A) Differences in metabolite abundance between control and mutant samples are represented as a volcano plot. Dashed vertical line represents a fold change (FC) of > 1.5. Dashed horizontal line represents $P < 0.01$. (B) A heat map illustrating the top 25 most significantly altered compounds in *Pyk*$^{60/61}$ mutants as compared with *Pyk*^{Prec} controls. Both figures were generated using Metaboanalyst 5.0, as described in the methods. Abbreviated compounds are 3-phosphoglycerate (3PG), 2-phosphoglycerate (2PG), phosphoenolpyruvate (PEP), 2-hydroxyglutarate (2HG), 3-hydroxybutyrate (2HB), alanine (Ala), Asparagine (Asn), Glutamic acid (Glu), Glutamine (Gln), 5'−Phosphoribosyl−N-formylglycinamide (FGAR), proline (Pro), trehalose (Tre).

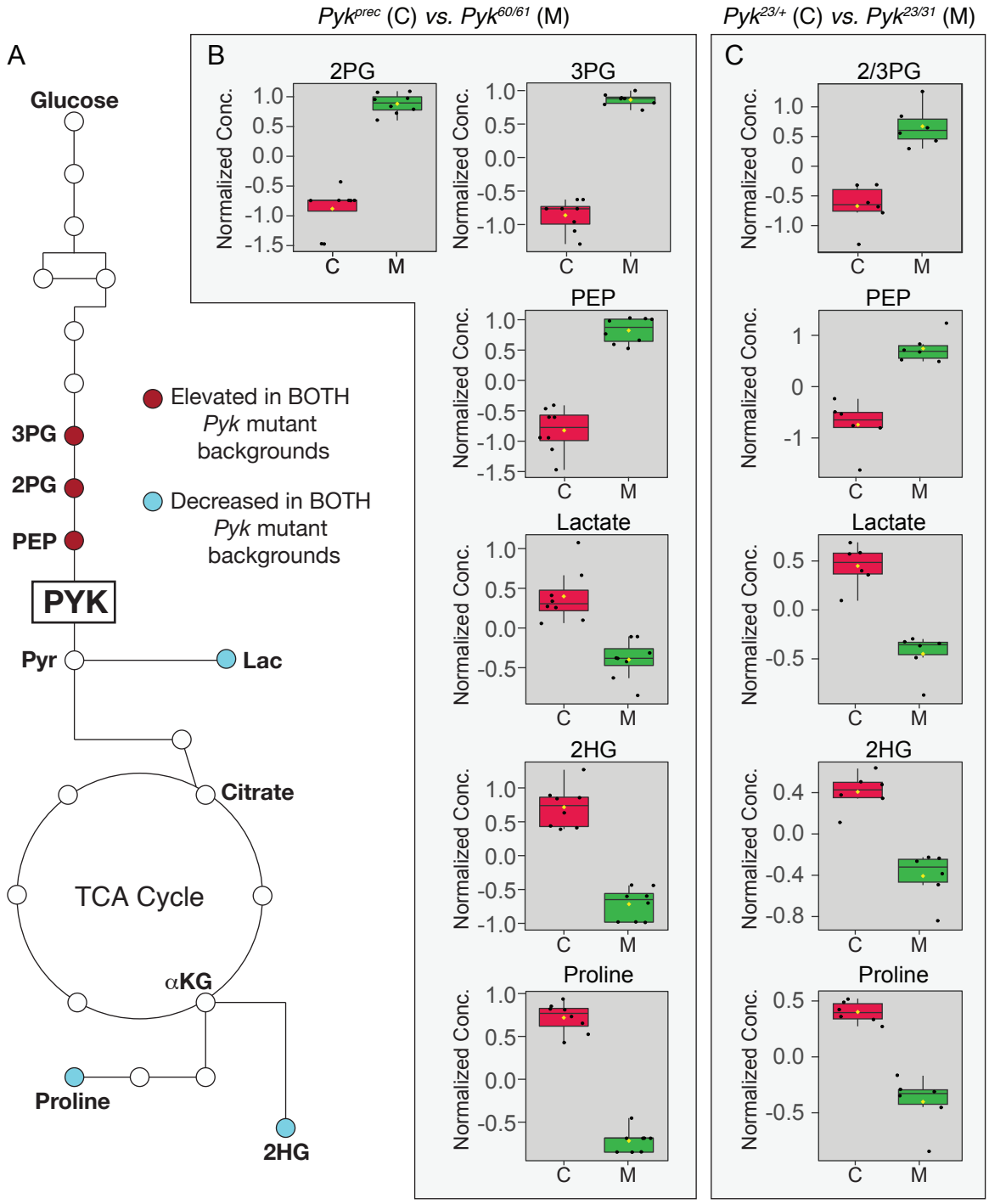

Figure 6. A limited set of metabolites are significantly altered in both *Pyk* mutant backgrounds. (A) An illustration of glycolysis and the TCA cycle with metabolites that are significantly altered in both *Pyk* mutant backgrounds highlighted in dark red (up-regulated) and light blue (down-regulated). (B,C) Boxplots illustrating the change in abundance of metabolites that are significantly altered in both (B) $Pyk^{23/31}$ and (C) $Pyk^{23/31}$ mutant backgrounds. All boxplots were generated using Metaboanalyst 5.0, as described in the methods. Black dots represent individual samples, the horizontal bar in the middle represents the median and the yellow diamond represents the mean concentration. For all boxplots, the metabolite fold-change was >2 fold and P>0.01. Abbreviated compounds are 3-phosphoglycerate (3PG), 2-phosphoglycerate (2PG), phosphoenolpyruvate (PEP), 2-hydroxyglutarate (2HG).

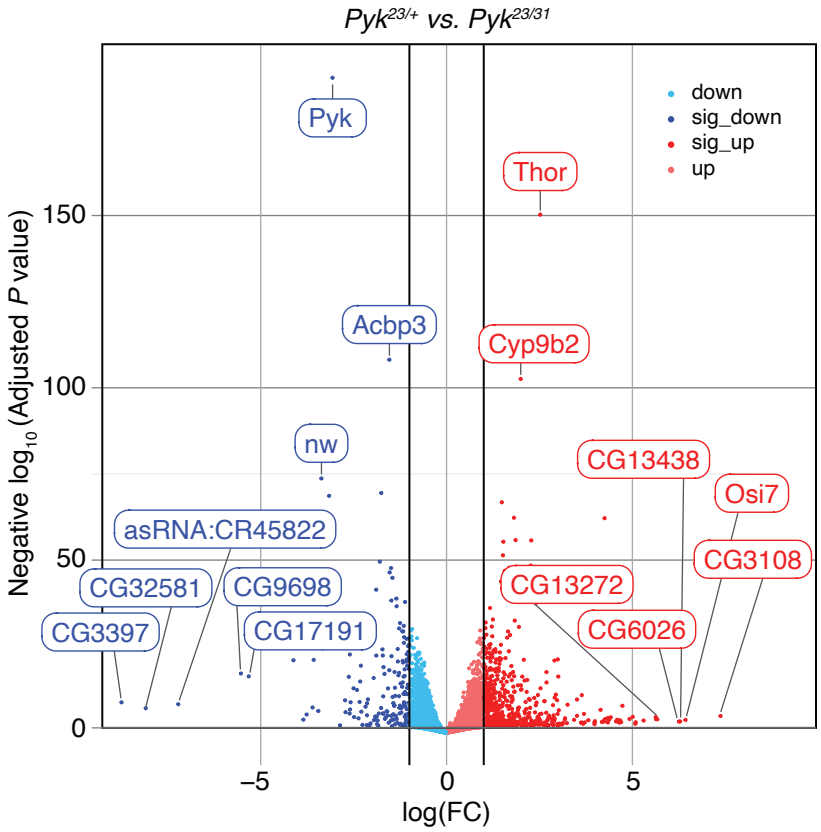

Figure 7. RNAseq analysis of *Pyk*$^{23/31}$ mutants as compared with *Pyk*$^{23/+}$ controls. A volcano plot illustrating gene expression changes in *Pyk*$^{23/31}$ mutants as compared with *Pyk*$^{23/+}$ controls. Vertical lines indicate log fold change (LFC). Horizontal lines represent adjusted *P* value. The top 15 most significantly changed genes are labeled.

A

Gene categories upregulated in *Pyk* mutants		
GO Category	Enrichment (N, B, n, b)	P-value
chitin metabolic process	3.45 (8151,101,421,18)	3.35E-06
lipid metabolic process	2.15 (8151,342,421,38)	5.51E-06
glucosamine-containing compound metabolic process	3.17 (8151,110,421,18)	1.16E-05
aminoglycan metabolic process	3.02 (8151,122,421,19)	1.39E-05
amino sugar metabolic process	3.11 (8151,112,421,18)	0.000015
cuticle development	2.66 (8151,160,421,22)	2.28E-05
fatty-acyl-CoA metabolic process	6.20 (8151,25,421,8)	2.35E-05
chitin-based cuticle development	2.64 (8151,154,421,21)	3.96E-05
fatty acid derivative metabolic process	5.74 (8151,27,421,8)	4.41E-05
lipid catabolic process	3.16 (8151,92,421,15)	0.000065
proteolysis	1.71 (8151,578,421,51)	9.53E-05
drug metabolic process	2.20 (8151,220,421,25)	0.000162
long-chain fatty-acyl-CoA metabolic process	8.07 (8151,12,421,5)	0.00021
regulation of chitin-based cuticle tanning	7.45 (8151,13,421,5)	0.000327
acyl-CoA metabolic process	4.19 (8151,37,421,8)	0.000486
thioester metabolic process	4.19 (8151,37,421,8)	0.000486
tyrosine metabolic process	8.60 (8151,9,421,4)	0.000718
central nervous system formation	8.60 (8151,9,421,4)	0.000718

B

Gene categories downregulated in *Pyk* mutants		
GO Category	Enrichment (N, B, n, b)	P-value
peptidyl-proline hydroxylation to 4-hydroxy-L-proline	27.70 (8151,11,107,4)	8.63E-06
4-hydroxyproline metabolic process	27.70 (8151,11,107,4)	8.63E-06
peptidyl-proline hydroxylation	27.70 (8151,11,107,4)	8.63E-06
protein hydroxylation	23.44 (8151,13,107,4)	1.83E-05
pyrimidine ribonucleoside monophosphate metabolic process	76.18 (8151,2,107,2)	1.71E-04
pyrimidine ribonucleoside monophosphate biosynthetic process	76.18 (8151,2,107,2)	1.71E-04
cellular amino acid metabolic process	5.04 (8151,121,107,8)	1.79E-04
response to organic substance	4.01 (8151,190,107,10)	1.85E-04
sensory perception of smell	8.86 (8151,43,107,5)	2.30E-04
peptidyl-proline modification	10.51 (8151,29,107,4)	5.18E-04
cellular modified amino acid metabolic process	5.86 (8151,78,107,6)	5.31E-04
alpha-amino acid metabolic process	5.57 (8151,82,107,6)	6.94E-04

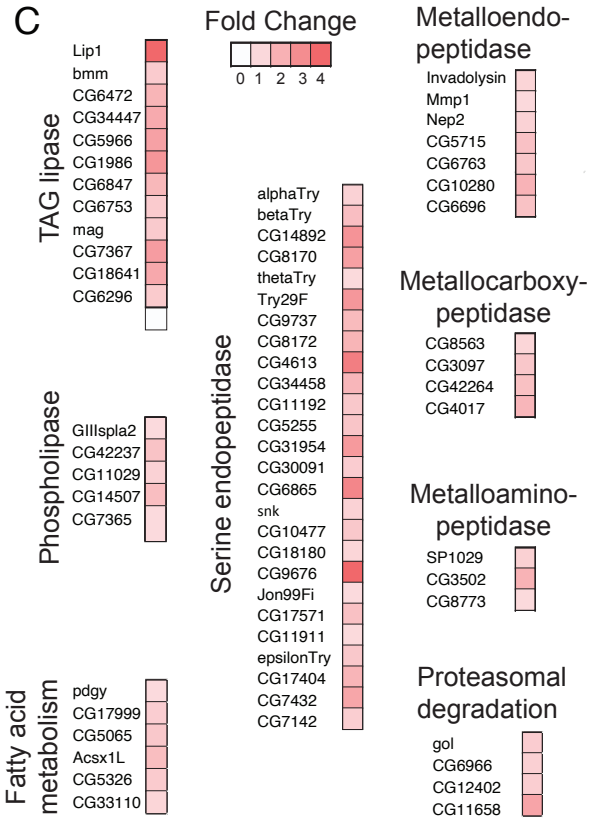

Figure 8. Gene Ontology (GO) enrichment analysis of genes that are significantly misregulated in *Pyk*$^{23/31}$ mutants. GOrilla was used to determine GO enrichment of biolog among those genes that were either (A) significantly up-regulated or (B) significantly down-regulated in *Pyk*$^{23/31}$ mutants when compared to the *Pyk*$^{23/+}$ control. (C) Significantly up-regulated genes in the GO categories "lipid metabolic process" and "proteolysis" are grouped by enzymatic function and the fold-change in gene expression is represented using a color gradient.